Estimation of Tidal Current in Tokyo-Ogasawara Area Using TOLEX-ADCP Data

Estimation of Tidal Current in Tokyo-Ogasawara Area using TOLEX-ADCP Data

Shoichi Kizu, Takeshi Taneda[1] and Kimio Hanawa

Department of Geophysics, Graduate School of Science, Tohoku University, Aoba-ku, Sendai 980-8578

Abstract : The tidal current in the sea between Tokyo and Ogasawara Islands is estimated by the harmonic analysis of the TOLEX-ADCP (Tokyo-Ogasawara Line EXperiment-Acoustic Doppler Current Profiler) data during 1991-1996. Four of the eight primary constituents (M_2, O_1, N_2 and Q_1) are reliably estimated. However, other three primary constituents (K_1, S_2 and P_1) are not properly estimated because of the infrequent sun-synchronous sampling characteristics of the measurement. K_2 tide is also excluded from the analysis considering its higher sensitivity to noises of semi-annual periodicity.

The average total tidal current of the four constituents (M_2, O_1, N_2 and Q_1) is about 10-20 cm/s in shallow water regions and 5 cm/s at largest elsewhere. The order of magnitude of the four constituents is $M_2 > O_1 > N_2 \geq Q_1$, which is consistent with nearby sea-level observations. The estimated tidal current is nearly vertically uniform from the surface to 400 m depth except in shallow water regions where it decreases substantially with depth. The obtained tidal constants of the four constituents agree with those of a global tidal model by Matsumoto *et al.* (1995) mostly within a few centimeter per second for the root-mean-squared current speed and about 30° for the tidal ellipse orientation.

Introduction

In recent years, the ship-mounted acoustic Doppler current profiler (ADCP) combined with precise measurements of ship's speed and heading has become popular as a tool for direct measurement of the ocean currents. The Physical Oceanography Group of Tohoku University installed a 150 kHz-type ADCP (RD Instruments, USA) on *Ogasawara-Maru*, the volunteer ship which weekly shuttles between Tokyo and Chichijima, Ogasawara Islands (Fig. 1), in 1990, and the oceanic flows in this area have been monitored by the equipment on a regular basis since February 1991 (Hanawa *et al.*, 1996). This is called TOLEX (Tokyo-Ogasawara Line EXperiment)-ADCP measurement. Our primary interest of the experiment is in non-tidal flows such as Kuroshio, so the tidal flow component needs to be separated from the ADCP-measured current velocity. Since the harmonic constants of tidal current are not published in the area, however, we estimate them based on our own velocity measurements in this paper.

The methodology of tidal analysis of ADCP measurements has been studied in many articles especially in coastal regions where tidal current dominates. Some of them used dynamical or statistical models of the oceanic tide (Foreman and Freeland, 1991 ;
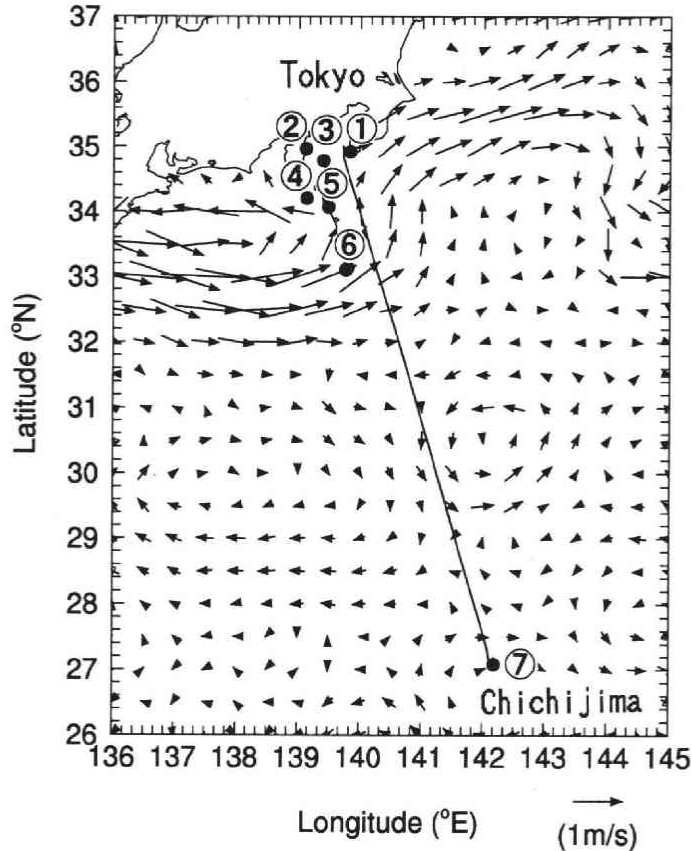
Fig. 1. The TOLEX-ADCP line (solid line) and a typical flow pattern (Dec. 14, 1997) estimated by the TOPEX altimetry (Yoshida *et al.*, 1997; arrows). Solid circles with numbers indicate the positions of nearby tidal observatories.

Candela *et al.*, 1992 ; Münchow *et al.*, 1992 ; Dowd and Thompson, 1996), and others were based on traditional harmonic analysis of the measured data (*e.g.* Geyer and Signell, 1990 ; Simpson *et al.*, 1990 ; Howarth and Proctor, 1992).

In the ordinary harmonic analysis, it is first necessary to determine the set of constituents to be estimated according to the length of record (*e.g.* Odamaki, 1981 ; Rikiishi, 1982).   Then the harmonic constants are estimated in a suitable mathematical way such as the least-square method.   This processing strategy is well-established in case of dealing with data taken by a regular and temporally-dense (*e.g.* hourly) sampling scheme.   However, this method is not readily applicable to data obtained from volunteer ships (VOS) whose sampling intervals vary largely in time.

The treatment of irregularly-sampled data in the harmonic analysis has partly been studied by authors (*e.g.* Rikiishi, 1982).   However, all sampling schemes discussed are random in time, which is not true for most VOS measurements that usually give sun-synchronous (*i.e.* not 'random") *and* infrequent sampling.   Unfortunately, our TOLEX

measurement is heavily suffered from this problem. No literature gives us a systematic way of processing of ADCP data obtained by such a temporally-biased sampling scheme.

Therefore, we firstly investigate which of the major constituents can be reliably estimated and which may not be, by a simple numerical analysis of various known noise-added artificial time series that are sampled by the TOLEX schedule. It is shown in the following that some of the primary tidal constituents (S_2, K_1, P_1 and K_2) are not likely be estimated with a good precision from our TOLEX-ADCP data. It is also shown that removal of the ill-defined constituents can seriously distort the estimation of non-tidal components. Based on these results, we estimate here only the constituents that are thought not to be influenced by the sampling deficit. Next, horizontal and vertical variation of the estimated tidal flow are described, and finally the results are compared to predictions by a global tidal model (Matsumoto *et al.*, 1995).

In Section 2, the TOLEX-ADCP measurement and data processing are outlined. In Section 3, the estimation of tidal current is briefly formulated based on the least-square method. The results are shown and their reliability is discussed in Section 4. Section 5 summaries and concludes this study.

2 TOLEX-ADCP measurement

The volunteer ship, *Ogasawara Maru* (3,553 t), was a cargo-passenger ship which almost weekly shuttled between Tokyo and Chichijima in the Ogasawara Islands (Fig. 1). It cruised at a speed of about 20 knots in the open ocean and connected the two ports, nearly 900 km apart, in about 29.5 hours for each way. The ship anchored at Tokyo for one night (nominally 17 hours) and at Chichijima for two or three nights (nominally 69 hours or 93 hours). In total, it usually took six or seven days for the ship to complete every return cruise. The ship repeated this cycle 58 times a year. Due to this cruising schedule, the time interval of measuring current at a fixed position was irregular and varies significantly depending on its location (Fig. 2). The ship was replaced by new *Ogasawara Maru* (6,679 t) in March 1997, and the ADCP measurement still continues with a new equipment installed by the Japan Marine Science and Technology Center (JAMSTEC).

The ADCP device was mounted at the bottom of the ship which was nominally 4m below the sea surface. The bin (*i.e.* vertical resolution) and the number of bins of the measurement were set to 16 m and 26, respectively, which yielded a vertical extent of measurement from near the surface to 420 m depth ($16\,\text{m} \times 26 + 4\,\text{m}$). The heading and speed of the ship were measured by an on-board gyrocompass and GPS (Global Positioning System), respectively. The ADCP data were smoothed and recorded every 5 minutes (300 pings). The time interval corresponds to a spatial resolution of about 3 km, according to the ship's speed.

In the post-processing, the data were spatially smoothed and projected onto points with 10-minute latitudinal intervals (27°10′N to 35°00′N) on a mean ship track, by using a Gaussian filter of which window width and e-folding scale were both 10 minutes in
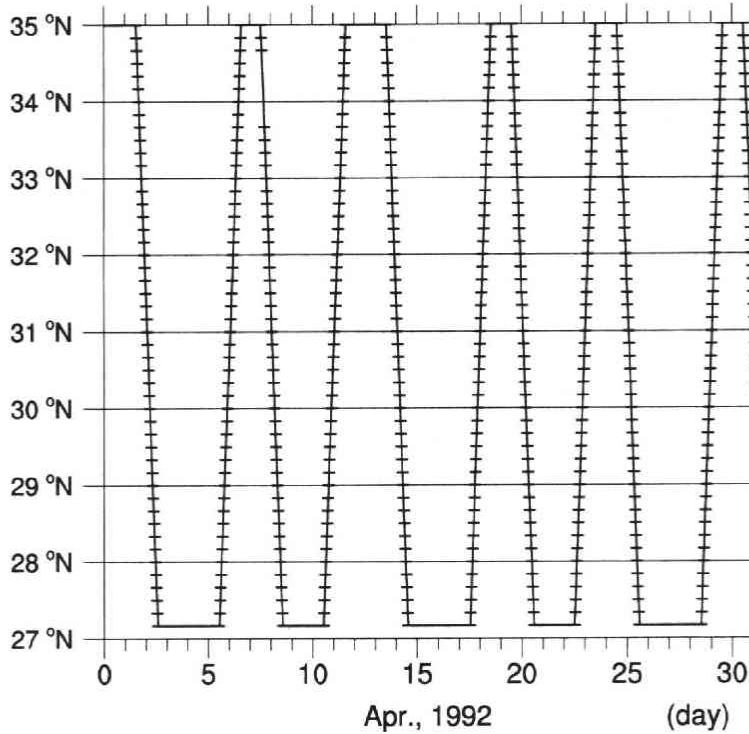
Fig. 2.   A typical sampling schedule of the TOLEX-ADCP measurement (April, 1992).
Slant lines show the ship's movement and horizontal short segments indicate the
times at which data are given.

latitude.   The longitudinal deviation of the ship track was less than 4 minutes.   Further
detail on the TOLEX-ADCP measurement and data processing can be found in Hanawa
et al. (1996) or Yoshikawa (1993).

The ADCP data obtained from February 1991 through November 1996 are used in
this study.   The total number of available data during the six years differs at different
locations but is approximately 490 per grid point, mostly varying from 5 to 10 per month.

In order to estimate the vertically-averaged tidal current, the ADCP data are
averaged over all of the 26 vertical bins in the most part of the analyses.   The vertical
structure of the tidal current is discussed in Section 5.

3   Method of tide-removal

The tidal current is estimated by the least-square method (Dronkers, 1964).   It's
eastward component, $u(t)$, is expressed as

$$u(t) = U_0 + \sum_i U_i \cos(\omega_i t - \chi_i) + \varepsilon(t) \tag{1}$$

where i refers to the each tidal constituent and N is the number of constituents considered. ω_i, U_i, χ_i are the angular velocity, the amplitude and the phase lag of the i-th constituent, respectively, and U_0 is the mean flow. $\varepsilon(t)$ is the residual between observed and estimated tidal current for a given time, and it consists of both the measurement error and non-tidal components of the velocity variation.

The mean-squared-residual is defined as

$$I(U_0, U_1, U_2, ..., U_N, \chi_1, \chi_2, ..., \chi_N) \equiv \sum_{j=1}^{n} \varepsilon(t)^2/n, \tag{2}$$

where n is the number of data and $\sum_j$ means summation over the total period of analysis. Then $2N+1$ simultaneous equations :

$$\frac{\partial I}{\partial U_0}=0, \frac{\partial I}{\partial U_i}=0 \quad (i=1, ..., N), \frac{\partial I}{\partial \chi_i}=0 \quad (i=1, ..., N) \tag{3}$$

are solved to minimize I, so that the $2N+1$ unknowns (U_0 ; $U_1, U_2, ..., U_N$; $\chi_1, \chi_2, ...,\chi_N$) are determined. The same procedure is applied to the meridional velocity component. Finally the results of both the components are combined to obtain tidal current vectors.

The nodal tide is neglected. Therefore, the tidal constants obtained here should be considered as average values over the total six-year period.

4 Results and discussions

4.1 Numerical pre-analysis

As previously mentioned, harmonic analysis of the six-year TOLEX-ADCP data could not identify some of the major constituents which should be properly estimated by temporally denser (e.g. hourly) sampling schemes. This is obviously due to the sun-synchronicity plus infrequency of the TOLEX-ADCP measurement. A typical example is S_2 tide which repeats with exact 12 hour period. Because the ship departed and arrived at the two ports at fixed times of a day except for occasional weather-induced delay, the sampled phase of S_2 tide at each grid point is highly confined (Fig. 3(a)). This does not happen in case of the other seven primary constituents (Fig. 3(b)). The biased sampling of S_2 tide is obviously a disadvantage for its proper identification.

In order to know impacts of this sampling deficit on the tidal analysis, a series of simple numerical experiments is performed. Investigated here is what happens if ordinary harmonic analysis is applied to various artificial (i.e. known) time series sampled by the TOLEX schedule at the presence of various "noise" (i.e. non-tidal) components.

The detail of the numerical experiments is given in Appendix A. Known facts are as follows. Firstly, S_2 tide is most poorly identified as expected. Inclusion of the constituent in the output components of the harmonic analysis can seriously distort the
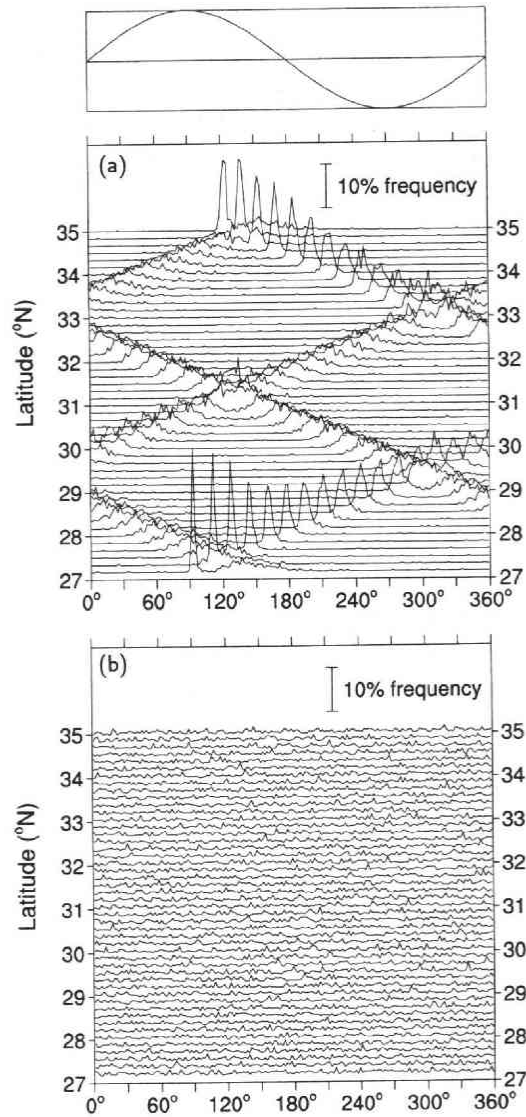
Fig. 3. Relative frequency of the sampled phases of (a) S_2 and (b) M_2 tide by the TOLEX schedule for each position on the route. Summarized in angular bins of two degrees. Frequency distribution of the other six primary constituents is virtually the same as that of M_2 tide.

estimation of non-tidal components. Secondly, K_1 and P_1 tides as well as S_2 tide are sensitive to various periodic noises, and also to a random noise to a lesser extent. Also, K_2 tide is sensitive to noises with semi-annual periodicity. This happens because the sun-synchronous TOLEX sampling scheme causes aliasing of the three (K_1, P_1 and K_2) constituents.

The actual TOLEX-ADCP data contains various periodic variations and random noise. It is impossible to precisely know their nature (*i.e.* periodicity, amplitude, etc.)

beforehand. Therefore, high sensitivity of the four constituents to possible non-tidal fluctuations let us decide to exclude them from the tidal analysis. It is shown in the next subsections that inclusion of these ill-definable constituents indeed gives us suspicious results.

4.2 General characteristics

The estimated ellipses of M_2, N_2, O_1, Q_1 tides are shown in Fig. 4(a), in which only the four constituents are considered as output. For comparison, calculation including all the eight primary constituents is also performed, and the result is presented in Fig. 4(b). A radial line in each tidal ellipse shows the current direction of each constituent at the local equilibrium tide. For most grid points and constituents shown in Fig. 4(a), the obtained tidal current vector rotates clockwise with time. The magnitude of the estimated current ellipse is larger at grid points in shallow water areas.

Table 1 shows amplitudes of sea level change due to the eight primary constituents measured at nearby tidal observatories. The estimated tidal constants for M_2, O_1, N_2 and Q_1 tides are presented in Table B1. Both the tables are obtained from the calculation including only the four reliably-estimated constituents. The order of magnitude of the tidal ellipses (Fig. 4(a)) and that of the amplitudes of sea level variation (Table 1) are consistent for M_2, O_1, N_2 and Q_1 tides. However, the obtained tidal currents of S_2 and P_1 tides are likely too large. K_1 and K_2 tides also appear to be overestimated (Fig. 4(b)).

4.3 Reliability

It is impossible to estimate errors of the present tidal analysis based on independent current measurement. Therefore, we investigate the robustness of the estimated tidal constants by comparing results obtained by choosing various combinations of output harmonics from the eight primary constituents. If we obtain stable results for a constituent regardless of the combination choices, we may consider that the estimation is successful.

The results are shown in Figs. 5-8, for each of the four major constituents (M_2, K_1, O_1 and S_2). For example, Fig. 5(a) gives estimated root-mean-squared current speed of M_2 tide defined by

$$\sqrt{\frac{1}{36}\sum_{j=1}^{36}\left|U_{M_2}\cos(\omega_{M_2}t_j - \chi_{M_2})\right|^2},$$ (4)

where U_{M_2}, ω_{M_2} and χ_{M_2} are the amplitude, the angular frequency and the phase lag of M_2 tide, respectively, and

$$t_j = \frac{j}{36}T_{M_2},$$ (5)

where T_{M_2} is the period of M_2 tide. Four different types of lines show the estimated values of M_2 tide in case of considering four combinations of harmonics as output (shown
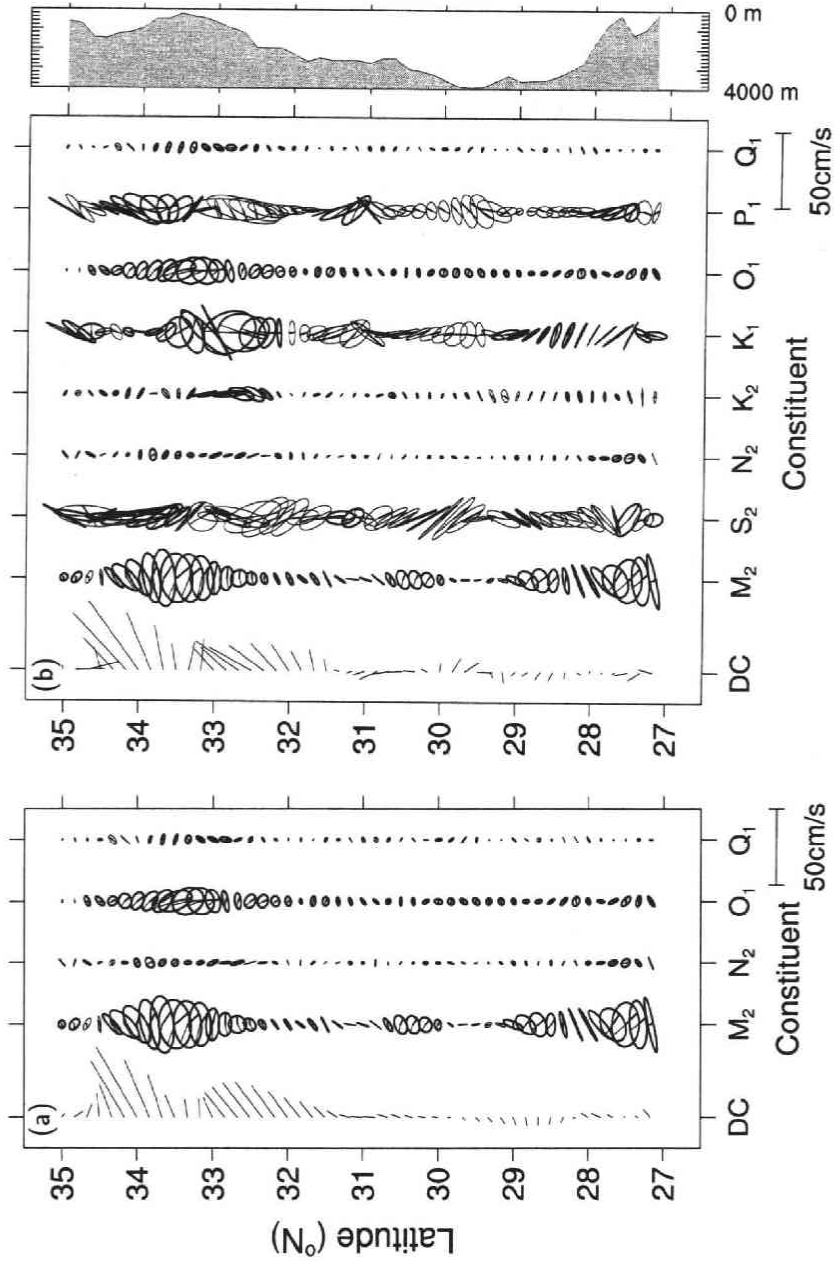
Fig. 4.   Tidal ellipses obtained by harmonic analysis applied to the TOLEX–ADCP data for two cases: (a) M_2, O_1, N_2 and Q_1 tides are included and (b) all eight primary constituents (M_2, K_1, O_1, S_2, P_1, Q_1, K_2, N_2) are included in the output.   Thick and thin ellipses respectively indicate clockwise and counter-clockwise rotation of the tidal current vectors.   A radial line in each ellipse shows the current direction at the local equilibrium tide.   "DC" stands for the mean flow.   The right panel shows the bottom topography along the ship track obtained from Terrain Base 5 minute mesh global terrain data (National Oceanic and Atmospheric Administration, 1995).

Table 1. Amplitudes of sea level change by eight major tidal constituents at tidal observatories near the TOLEX-ADCP track. Amplitudes for all except M_2 tide are given in magnitude relative to M_2 tide.

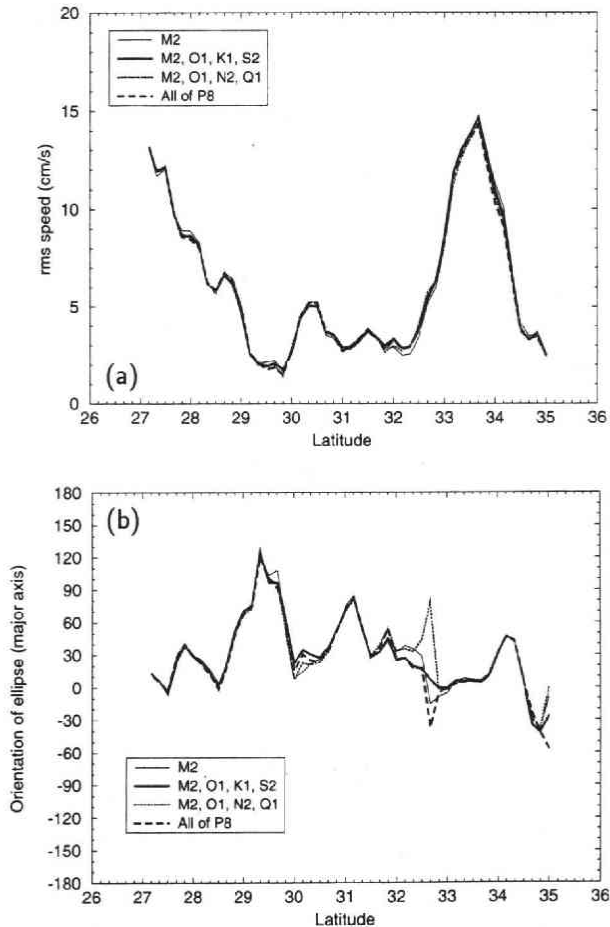| site name	No.	M_2 (cm)	M_2 (%)	K_1 (%)	O_1 (%)	S_2 (%)	P_1 (%)	N_2 (%)	K_2 (%)	Q_1 (%)
Mera	①	36.0	100.	63.9	50.3	46.9	21.1	14.7	13.1	10.3
Ito	②	35.2	100.	67.2	52.3	46.6	21.6	15.6	12.5	10.5
Okada	③	35.1	100.	65.8	51.9	47.0	21.4	15.1	12.8	10.5
Kozu-shima	④	38.3	100.	58.5	45.4	46.5	18.8	15.7	12.8	9.7
Ako	⑤	34.7	100.	65.1	50.4	47.3	21.3	15.9	12.7	10.4
Kaminato	⑥	31.6	100.	58.2	45.6	47.5	18.0	14.6	11.1	9.3
Futami	⑦	28.3	100.	57.6	42.4	45.6	18.7	18.4	12.4	8.1

Fig. 5. Comparison of estimated tidal ellipse parameters of M_2 tide for various combinations of constituents as output. a) Root-mean-square speed (cm/s) and b) orientation of major axis (degree). Different line types indicate results obtained for different combinations of constituents considered (see legend). The angular parameters are counter-clockwise positive from the east.

in the legend), respectively.   Fig. 5(a), shows the orientation of the major axis of the M_2 tidal ellipses for the same choices of output.   Figs. 4-8 are similar comparisons for the estimated parameters of O_1, K_1 and S_2 tide, respectively.

The constants of M_2 and O_1 tides are insensitive to changing the combination of constituents (Fig. 5-6) though those of S_2, K_1 (Fig. 7-8) and P_1 (not shown) tides are not. The estimated parameters of M_2 tide are almost always the same except for some deviations in the area where tidal current is weak (near 32°N and 35°N ; see Fig. 4 and Fig. 5(a)-(b)).   The parameters of O_1 tide (Fig. 6) are also stable.   In contrast, however, the obtained ellipse parameters of K_1 (Fig. 7) and S_2 (Fig. 8) tides are sensitive to the choice of harmonics combination.   The result of K_1 tide depends clearly on whether P_1 tide is included or not in the output harmonics.

The tidal ellipses of M_2 and O_1 tides vary more continuously along the shiptrack than those of S_2, K_1 and P_1 tides do (Fig. 4(a) and Fig. 4(b)).   This is realistic considering that the tidal variation in this area basically behaves like a very long wave.   The
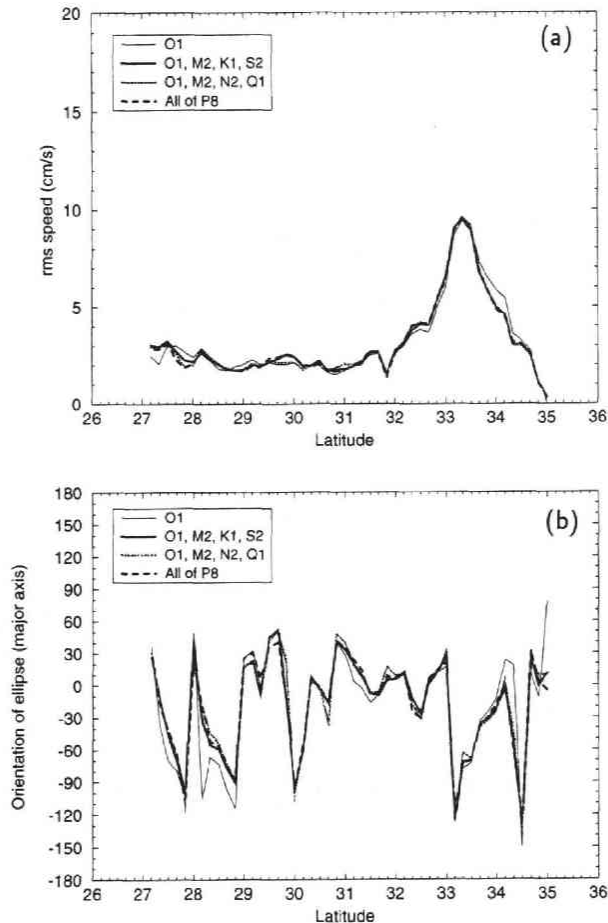

Fig. 6.   Same as Fig. 5 but for O_1 tide.
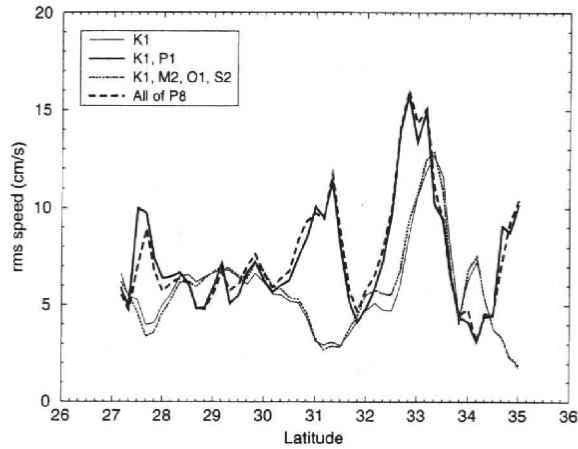
Fig. 7.   Same as Fig. 5(a) but for K_1 tide.
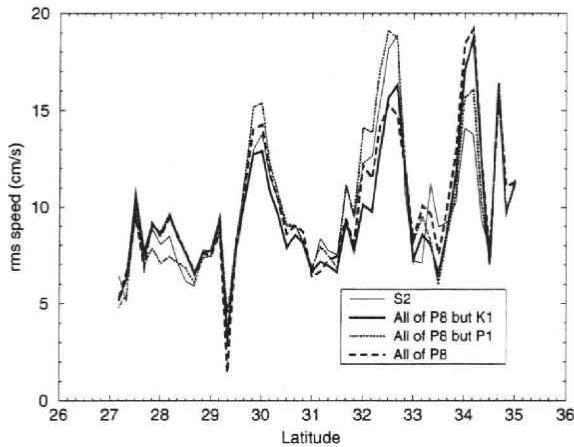
Fig. 8.   Same as Fig. 5(a) but for S_2 tide.

robustness and the spatial continuity of the estimated tides suggest that the four of the eight primary constituents (M_2, O_1, N_2 and Q_1) are reliably estimated whereas S_2, K_1 and P_1 tides are not.   The validity of the estimated K_2 tide is not clear from only these points of view, but we also exclude the constituent from the analysis considering its high sensitivity to possible semi-annual components of the velocity fluctuation.

4.4   Vertical structure

We estimated the vertically-averaged tidal current so far in the present study.   This is practically because more variant results tend to be obtained by analyses of data containing smaller number of bins.   The vertical averaging may also be supported by the large sea depth for most part of the area, where internal tide is not likely prevalent. Here, however, the analysis is applied separately to sub-layers containing fewer bins in order to check the assumption of vertical uniformity of motion.   Fig. 9(a) and Fig. 9(b)
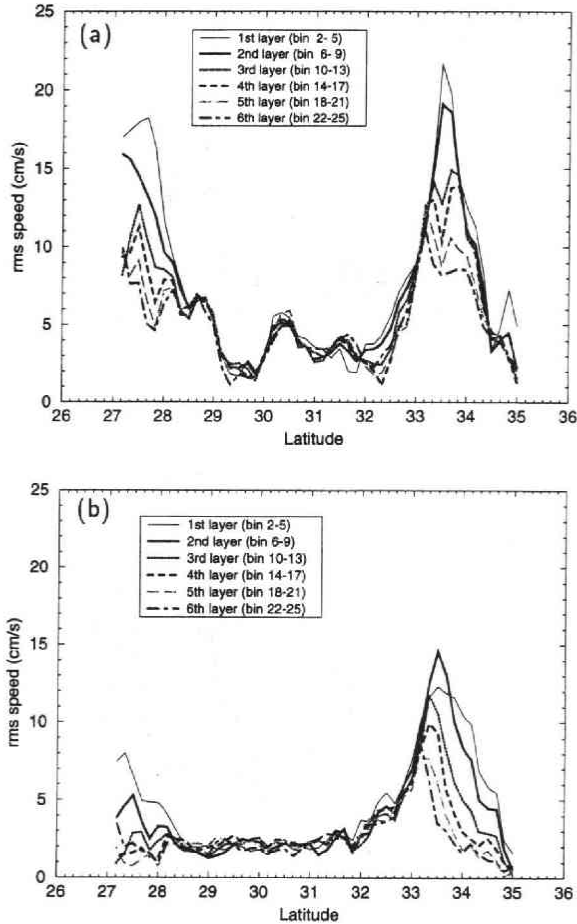
Fig. 9. Comparison of the root-mean-square current speed of (a) M_2 tide and (b) O_1 tide in six vertical sub-layers. Numbers of bins in the legends are from the shallowest (bin 1) to the deepest (bin 26).

show latitudinal variation of the root-mean-squared speed of M_2 and O_1 tide, respectively, in six vertical sub-layers. Each sub-layer consists of 4 bins (about 64 m thickness).

The tidal current decreases substantially with depth in shallow water areas near 33.5°N and 27.5°N. The flow structure suggests that the vertical averaging may be inadequate in these regions. In contrast, the estimated tidal current is vertically uniform in the rest of the area where the sea depth (Fig. 4) is much greater, and hence our estimation should be a good approximation there. Since the ill-definition of the four constituents (S_2, K_1, P_1 and K_2) is not confined to the shallow water areas, the problem is not likely caused by the vertical inhomogeneity of the tidal current.

4.5 Sum of the four tidal constituents

The root-mean-squared speed of the estimated tidal current (sum of M_2, O_1, N_2, Q_1) is shown in Fig. 10. The sum of the four constituents is about 10-20 cm/s in the shallow

Fig. 10. The root-mean-square speed of raw ADCP-measured current (thin solid line), sum of the estimated tidal current (M_2, O_1, N_2 and Q_1 ; thick solid line), and tide(only the four constituents)-removed current (dotted line).

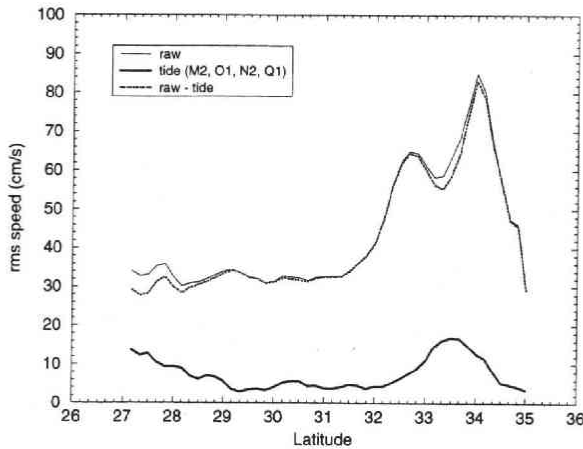water areas and 5 cm/s at largest elsewhere. According to the nearby sea level observations (Table 1), the reliably estimated four constituents share more than a half of the total tidal variability in this area. Therefore, it is inferred that the total tidal current is O (10 cm/s) in Tokyo-Ogasawara area except in the shallow water regions. It is also expected that more than a half of the total tidal current variability can be removed if we subtract the sum of the four constituents from the ADCP-measured velocity.

4.6   Comparison to a global tide model

Currently there is no regional tidal model available with detail bottom topography that allows us to precisely predict tidal current in the area of TOLEX measurement. Fortunately, however, many global tidal models, despite calculated based on coarse topography, have become available with the aid of TOPEX altimetry in recent years. Here our tidal estimation is briefly compared with that computed by one of such global tide models, by Matsumoto *et al.* (1995), which we refer to as NAO (National Astronomical Observatory) model hereafter. The Fortran source code of the model is available from a CD-ROM by the Physical Oceanography Distributed Active Archive Center (PO-DAAC), the Jet Propulsion Laboratory (http://podaac.jpl.nasa.gov/cdrom/tide/index. htm), but its ordinary use provides only the tidal sea level prediction. We are allowed to use the corresponding tidal current data by favor of the author (Matsumoto, personal communication).

Fig. 11-12 show comparisons of the ellipse parameters of M_2 and O_1 tides by our estimates and the computation by the NAO model. The two estimates agree well for the size of M_2 tidal ellipses (Fig. 11(a)) except that the model estimation is slightly smaller in the shallow water areas. The two estimates of the ellipse orientation (Fig. 11(b),) and the current direction at the equilibrium high tide (Fig. 11(c)) differ as much as 90° in the areas of weak current. However, much better agreement is obtained else-
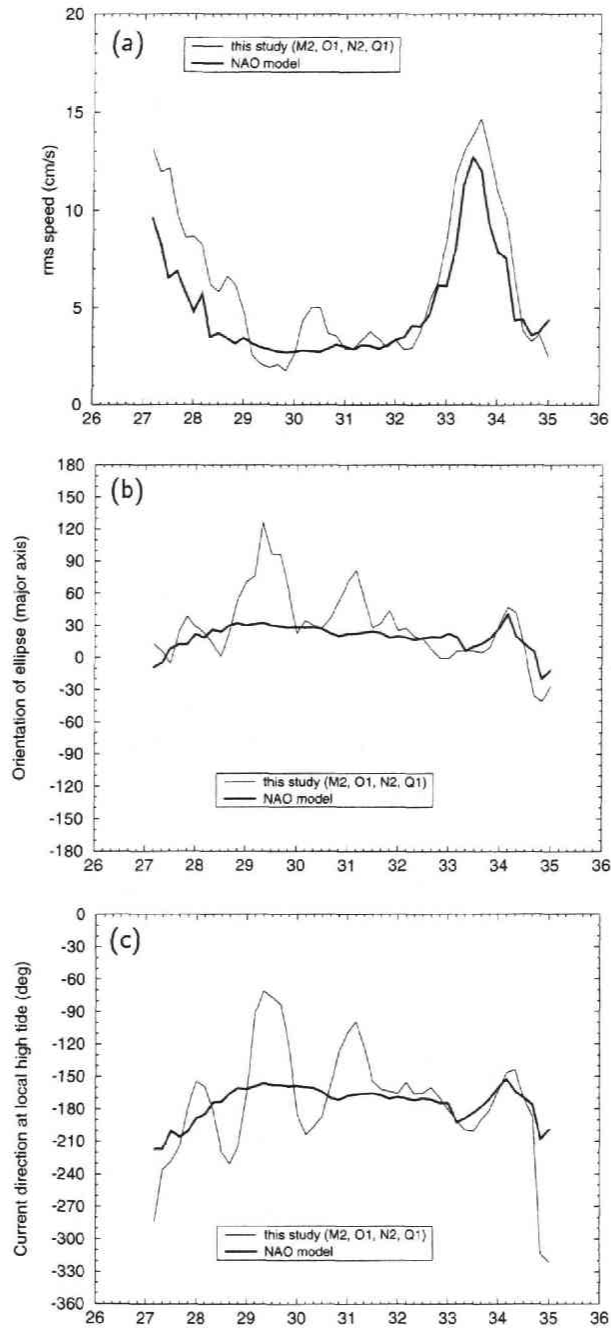
Fig. 11. Comparison of the estimates of tidal ellipse parameters by this study and those by NAO model for M_2 tide. (a) Root-mean-square speed, (b) orientation of ellipse, and (c) current direction at local high tide. Definitions of the angular parameters are the same as Fig. 5.
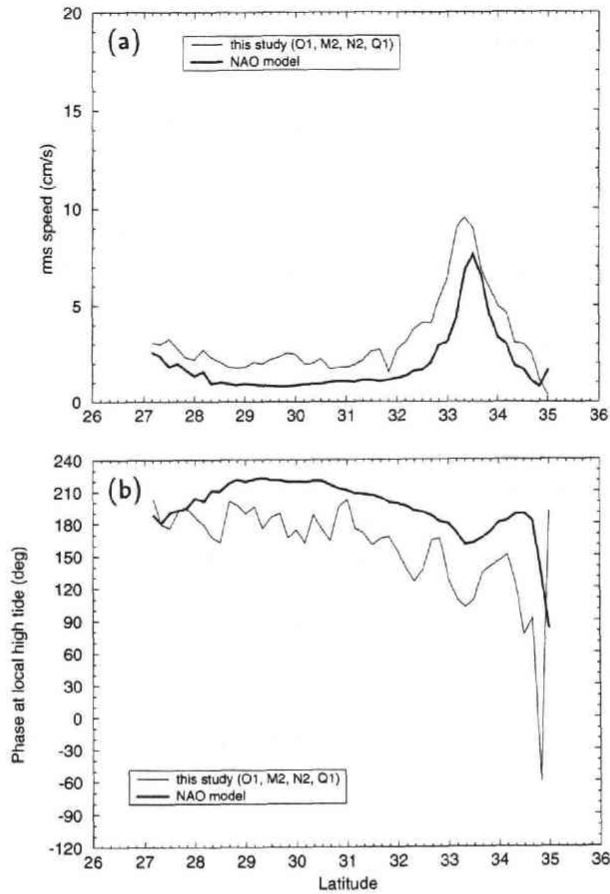
Fig. 12.   Same as Fig. 11 but for O_1.   (a) Root-mean-square speed and (b) current
direction at local high tide.

where.   The difference between our estimate and that of the NAO model in the deep
water area is mostly a few centimeter per second for the rms current speed and 30° for
the major axis orientation in the area with appreciable current speed.

The longer axis of the ellipse lies grossly in zonal (east-west) direction in both the
estimates, and the tidal current is westward at local high tide (Fig. 11(c)).   Considering
that M_2 tidal wave propagates westward in this area (e.g. Schwiderski, 1980), these
angular relationships may support the fact that M_2 tidal wave is basically progressive in
this area.

In case of O_1 tide, however, the agreement between the two estimates is generally
worse.   Our estimate of the size of ellipse is larger than that by the NAO model (Fig.
12(a)), and the current direction at local high tide by the model is systematically larger
than our estimate by about 30° (Fig. 12(b)).   The reason of these disagreements is not
clear, but either or both of the model and our estimate may need future improvement.

5 Summary and conclusions

The tidal current in the area between Tokyo and Ogasawara Islands is estimated by a harmonic analysis of the TOLEX-ADCP data. M_2, O_1, N_2 and Q_1 tides are reliably estimated. K_1, S_2 and P_1 tides are not, however, mainly because of the sun-synchronous under-sampling scheme of the measurement. K_2 tide is not estimated either, considering its high sensitivity to possible semi-annual variations in the flow field. It should be noted that this problem is not thought to be limited to our TOLEX case but may occur in case of similar (*i.e.* sun-synchronous and infrequent) sampling schemes.

The amplitudes of the estimated tidal current is larger in the shallow water areas (near Hachijo-jima (33°N) and the north of Chichijima (28°N)), and the current direction at the local high tide is mostly west-southwestward. These are reasonable if the progressive-wave-like behaviour of the oceanic tide is assumed in this region. It is also shown that the tidal current is nearly vertically uniform in the top 400 m layer, except in the shallow water regions where it substantially decreases with depth.

We also compared our results to predictions by the global tide mode by Matsumoto *et al.* (1995), and obtained reasonable agreements in deep parts of the area. Our estimate and that of the NAO model differ mostly as much as a few centimeter per second for the rms current speed and 30° for the major axis orientation. However, disagreements are found in the shallow water areas, suggesting that either or both of our estimates and the tidal model prediction should be improved in these shallow water regions.

The average total current of the estimated four constituents (M_2, O_1, N_2 and Q_1) is 10-20 cm/s in the shallow water areas and 5 cm/s at largest elsewhere. Comparing to the nearby sea level measurements, it is inferred that more than a half of the total tidal variability can be removed by subtracting the sum of these four constituents from the ADCP-measured velocity.

Appendix A

The artificial time series used in the numerical analysis are commonly expressed by

$$V(t)=\sum_{i=1}^{8}A_i\cos(\omega_i l+\phi_i)+B\cdot F(t) \tag{A1}$$

where i represents each of the eight primary tidal constituents considered here (M_2, K_1, O_1, S_2, P_1, N_2, K_2, and Q_1). A_i, ω_i, ϕ_i are the amplitude, the angular frequency and the initial phase of the i-th tidal constituent, respectively. For simplicity, all A_i's are taken as unity and all ϕ_i's are taken as zero. The value of B is set to 1, 2, 5, 10, 15 and 20 in individual runs to investigate how error depends on the amplitude of the noises.

The "non-tidal" part of the input signal, $F(t)$, which plays a role of noise in the computation, is specified differently in different cases. In Case 1, a *random* noise is given as $F(t)$:

$$F(t)=\text{a series of pseudo random numbers between }-1\text{ and }1. \tag{A2}$$

Case 2 consists of two thousand runs in each of which a single but various periodic function is given as $F(t)$:

$$F(t)=\cos(\Omega t+\Phi), \tag{A3}$$

where Ω and Φ are taken as constants. Two thousand Ω's are chosen randomly in a wide spectral range from sub-daily to nearly 500 days, each of which is given with random Φ in the individual run of Case 2. This type of noise is referred to as *periodic* noise in the following.

The artificial time series are sampled by each of the two following schemes : 1) six year TOLEX schedule and 2) one year hourly sampling. Then the harmonic analysis based on the least-square method is applied to each of the discrete records. Here the eight primary constituents are considered as output.

The results of the experiments are summarized in Table A1 and partly illustrated in Fig. A1. In Table A1, root-mean-squared difference between the input (given) and output (obtained) constituent :

$$\frac{I}{n_j\times n_k}\sum_{j}^{n_j}\sum_{k}^{n_k}(A_i\cos\phi_i-A'_{ik}\cos\phi'_{ik})^2, \tag{A4}$$

where A'_{ik} and ϕ'_{ik} are amplitude and phase of the output, is shown for each tidal constituent and value of B. n_j and n_k are the number of latitudinal grid points ($n_j=48$) and the number of runs with different pseudo random number series ($n_k=19$), respectively. n_j times n_k gives the total number of cases to to calculate the rms error for each

Table A1.   Root-mean-squared error of harmonic analysis for each of the
eight primary constituents of Case 1 artificial time series sampled by
TOLEX measurement schedule (unparenthesized) and hourly sam-
pling (parenthesized).   Values are given in the unit of percent.

	$B=1$	$B=2$	$B=5$	$B=10$	$B=15$	$B=20$
Q_1	3 (0)	6 (1)	15 (2)	31 (5)	46 (7)	62 (9)
O_1	3 (1)	6 (1)	15 (3)	29 (6)	44 (8)	58 (11)
P_1	5 (0)	11 (1)	27 (1)	54 (3)	81 (4)	109 (5)
K_1	5 (1)	10 (2)	25 (5)	49 (10)	74 (16)	98 (21)
N_2	3 (0)	6 (0)	16 (1)	32 (1)	48 (2)	65 (3)
M_2	3 (0)	6 (1)	16 (2)	31 (3)	47 (5)	62 (7)
S_2	8 (1)	16 (2)	39 (5)	79 (10)	118 (14)	158 (19)
K_2	3 (1)	6 (1)	15 (3)	31 (6)	46 (9)	61 (12)

constituent and noise amplitude.

Fig. A1 indicates amplitude errors of the eight constituents for Case 2 for a site with typical sampling schedule.   It shows that S_2, K_1 and P_1 tides are preferably distorted by contamination of a wide range of periodic noise. K_2 tide is also affected by some periodic noise, but the effective ones are mostly confined to semi-annual band.   The other four constituents (M_2, O_1, N_2 and Q_1) are not significantly influenced by contamination of various periodic noise.

Why are S_2, K_1 and P_1 tides poorly estimated?   As shown in Fig. 3(a), the pseudo sun-synchronicity plus frequency of the measurement highly confines the range of sampled phase of S_2 tide at each point.   This biased sampling of S_2 tide is undoubtedly a deficit for its proper identification.

K_1 (period $T=23.93$h), P_1 ($T=24.07$h), and K_2 ($T=11.97$h) tides have another scenario.   In a multi-year period, almost whole range of phase is sampled for these three constituents.   However, since K_1 and P_1 tides have periodicity close to one day, their sampled phases shift very gradually and complete one cycle during a year.   In other words, the TOLEX sampling of the two constituents causes aliasing of one year.   Similarly, K_2 tide has a aliased period of half a year.   The fact that the three constituents are more sensitive to the contamination of "noise" with annual (for K_1 and P_1 tides) and semi-annual (for K_2 tide) periodicity is consistent with this possibility of aliasing.   The duration of the TOLEX-ADCP measurement is long enough to seperate the eight primary tidal constituents by using hourly-sampled data, but the temporally-biased TOLEX sampling scheme can cause aliasing and yield errorneous results in detecting these constituents at the presence of various noises.

The actual TOLEX-ADCP record should contain various types of periodic variations and random noise, which may not be fully represented by the two types of "noises", purely periodic and purely random, treated here.   However, such non-tidal components in the real record can be considered as a mixture of them.   The facts that S_2, K_1, P_1 tides are sensitive to the contamination of both types of noises and that the results of the three are indeed more doubtful than those of the other major constituents from various aspects
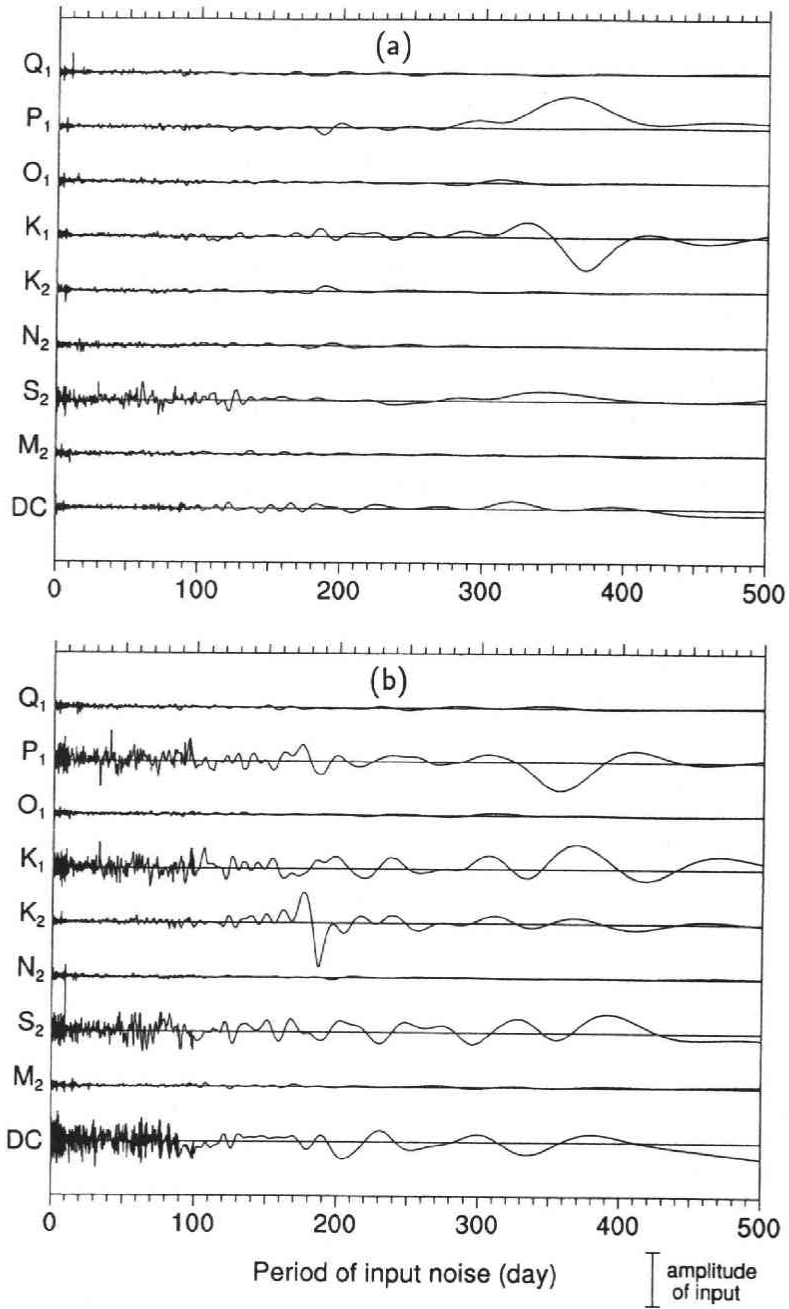
Fig. A1. Difference of the input and output amplitudes (output minus input) of each
constituent of the Case 2 signal sampled by the TOLEX schedule. Abscissa
shows the period of input noises (see the text). (a) 32°00′N and (b) 33°00′N.

suggest that the sun-synchronous infrequent sampling scheme by the TOLEX measurement can significantly distort the estimation of the three constituents. The result of K_2 tide is also considered to be somewhat less reliable than the rest of the eight primary constituents (M_2, O_1, Q_1 and N_2) because of its higher sensitivity to the contamination of semi-annual noise, though it seems to be more stably identified than the former three constituents (S_2, P_1 and K_1).

It is very difficult to make quantitative estimation of errors for individual tidal constituents, since the magnitude of error largely depends on the signal-to-noise ratio (*i. e.* value of A/B) which is not known in the real ocean. However, if we assume that the results of four tides (M_2, O_1, Q_1 and N_2) are correct and use them to estimate the non-tidal (strictly, including unestimated tidal components) variability, the value of B/A is likely less than 5 for M_2 tide and may be larger than 10 for minor constituents (*e.g.* Q_1 and N_2). Therefore, we infer that the error of tidal estimation made in this study is approximately 15-20% for the major constituents (M_2 and O_1) and possibly more than 30% for the minor constituents (Q_1 and N_2).

Appendix B

The tidal constants of M_2, O_1, N_2 and Q_1 tides are presented in Table B1. They are estimated by including only these four reliably-estimated constituents as output.

Table B1. Tidal current constants of M_2, O_1, N_2 and Q_1 constituents estimated by harmonics analysis of the six-year TOLEX-ADCP data. Latitude (degree), maximum and minimum current speeds, U_{max} and U_{min} (cm/s), respectively, direction of maximum current speed, θ_{max}, and current direction at local equilibrium tide (degree), Θ. The angles are counter-clockwise positive from the east. (a) M_2 tide, (b) O_1 tide, (c) N_2 tide and (d) Q_1 tide.

(a) M_2 tide.

latitude	U_{max}	U_{min}	θ_{max}	Θ	latitude	U_{max}	U_{min}	θ_{max}	Θ
35.000	2.7	2.3	−0.7	−174.5	31.000	4.1	0.2	−109.0	70.3
34.833	4.2	2.8	−38.3	176.5	30.833	5.0	0.2	−127.5	53.7
34.667	4.5	1.7	−29.3	63.2	30.667	5.0	1.7	−147.3	8.6
34.500	5.3	0.9	−174.3	19.9	30.500	6.4	3.9	−156.3	−23.6
34.333	8.9	2.3	−137.5	18.0	30.333	6.0	4.3	−159.1	−32.4
34.167	12.4	5.0	−132.7	2.2	30.167	4.9	4.2	−157.3	−41.0
34.000	13.9	6.0	−147.4	−13.7	30.000	3.5	2.1	−172.4	−25.4
33.833	16.7	5.9	−167.4	−26.2	29.833	2.0	0.1	−126.8	49.5
33.667	18.8	7.5	−174.0	−33.7	29.667	2.8	0.1	−84.9	94.9
33.500	16.0	10.4	−173.2	−49.9	29.500	2.7	0.6	−79.4	96.8
33.333	15.4	9.0	−173.9	−48.2	29.333	2.4	1.5	−55.4	110.1
33.167	14.2	7.2	−176.8	−34.0	29.167	3.7	0.9	−107.9	93.2
33.000	10.6	4.4	177.4	−13.1	29.000	6.9	2.1	67.9	1.5
32.833	7.6	4.6	178.5	−2.8	28.833	7.8	4.8	49.7	−37.0
32.667	6.0	5.5	78.9	2.6	28.667	8.1	5.2	19.9	−47.7

latitude	U_{max}	U_{min}	θ_{max}	Θ	latitude	U_{max}	U_{min}	θ_{max}	Θ
32.500	4.6	3.4	−136.2	9.3	28.500	7.4	3.1	−179.3	−35.2
32.333	3.7	1.8	−147.2	12.9	28.333	8.7	1.4	−165.5	2.9
32.167	3.8	0.5	−144.7	29.1	28.167	11.5	0.4	−156.0	22.1
32.000	4.1	0.9	−146.4	13.1	28.000	12.1	0.7	−150.2	24.7
31.833	3.7	0.6	54.4	−21.5	27.833	12.0	3.0	40.2	2.0
31.667	4.7	1.2	−141.1	4.4	27.667	11.6	7.6	−151.2	−21.8
31.500	5.5	0.3	−151.1	22.8	27.500	14.5	9.0	177.2	−44.1
31.333	4.6	0.6	−126.1	59.7	27.333	15.9	5.6	5.2	−45.4
31.167	4.0	0.2	−99.9	81.0	27.167	18.5	1.9	12.1	−39.7

(b) O_1 tide.

latitude	U_{max}	U_{min}	θ_{max}	Θ	latitude	U_{max}	U_{min}	θ_{max}	Θ
35.000	0.5	0.2	9.7	3.4	31.000	2.8	0.8	−140.6	15.8
34.833	1.5	0.0	−171.0	−176.5	30.833	2.5	0.7	−131.6	−5.6
34.667	3.5	1.6	−156.8	−123.5	30.667	1.9	1.6	−38.2	−29.8
34.500	3.9	1.8	−136.9	−117.9	30.500	2.9	0.6	−1.3	−5.4
34.333	3.4	2.9	−41.1	−68.2	30.333	2.5	1.1	5.6	2.3
34.167	5.0	4.2	−175.4	−47.4	30.167	2.2	1.2	−55.9	−28.2
34.000	6.1	3.7	−24.5	−51.8	30.000	2.5	1.7	−102.8	−15.8
33.833	7.4	4.0	−33.8	−52.5	29.833	2.3	2.0	−154.0	−20.3
33.667	8.5	5.0	−38.6	−57.6	29.667	2.6	1.5	−127.1	6.7
33.500	11.3	6.0	−68.1	−78.6	29.500	2.7	1.7	−140.4	−2.5
33.333	10.6	8.5	−63.3	−87.8	29.333	2.3	1.7	−5.2	−11.7
33.167	9.3	8.5	−126.6	−83.0	29.167	2.4	1.8	20.6	5.8
33.000	7.7	4.8	−162.9	−69.8	29.000	2.1	1.3	18.5	0.9
32.833	7.2	1.9	−168.0	−21.2	28.833	2.1	1.3	−88.7	0.3
32.667	5.3	2.1	−172.8	−24.0	28.667	2.3	1.3	−72.6	4.2
32.500	4.8	3.5	−27.3	−54.9	28.500	2.8	0.9	−53.6	−26.4
32.333	4.4	3.4	161.8	−70.0	28.333	3.3	1.2	−43.8	−18.6
32.167	3.6	2.7	−169.2	−67.2	28.167	3.3	2.3	−19.6	−3.3
32.000	3.3	2.0	−171.1	−47.8	28.000	2.4	1.4	19.8	0.8
31.833	1.8	1.0	−162.5	−33.8	27.833	2.5	1.1	−99.1	−13.3
31.667	3.4	1.7	−6.0	−21.3	27.667	3.5	1.1	−63.3	−31.7
31.500	3.0	2.3	−6.9	−31.9	27.500	4.1	1.9	−44.1	−16.3
31.333	2.8	1.2	−172.2	−21.2	27.333	3.8	1.6	−12.5	−5.5
31.167	2.7	1.0	−161.7	−18.7	27.167	4.0	1.2	31.2	21.0

(c) N_2 tide.

latitude	U_{max}	U_{min}	θ_{max}	Θ	latitude	U_{max}	U_{min}	θ_{max}	Θ
35.000	3.4	0.4	−140.3	−133.6	31.000	0.9	0.8	155.9	121.3
34.833	2.2	0.0	162.3	162.3	30.833	2.1	0.0	177.6	177.4
34.667	2.9	0.6	58.3	39.3	30.667	1.3	0.1	−173.5	−172.0

latitude	U_{max}	U_{min}	θ_{max}	Θ	latitude	U_{max}	U_{min}	θ_{max}	Θ
34.500	1.7	0.6	111.3	156.6	30.500	1.3	0.2	146.7	152.7
34.333	2.2	1.5	133.2	−171.5	30.333	0.8	0.4	130.7	−46.6
34.167	2.0	0.9	88.8	−72.6	30.167	1.4	1.0	91.8	−50.2
34.000	2.9	1.7	20.8	−59.3	30.000	1.3	0.7	87.3	−18.4
33.833	3.6	2.5	31.9	−85.5	29.833	1.9	0.4	71.3	17.4
33.667	2.7	1.8	−38.9	−67.5	29.667	1.1	0.2	68.6	−76.3
33.500	2.4	2.1	−21.0	−73.0	29.500	1.3	0.3	104.2	−120.5
33.333	2.3	1.3	92.2	−75.6	29.333	0.4	0.2	29.8	11.3
33.167	2.4	1.2	106.7	−41.6	29.167	1.1	0.4	47.7	36.5
33.000	3.8	1.2	114.0	−38.1	29.000	1.5	0.9	34.3	−12.8
32.833	3.6	0.7	95.9	36.6	28.833	1.4	0.3	13.9	2.3
32.667	4.5	1.0	105.0	87.5	28.667	1.6	0.2	−11.7	34.8
32.500	4.4	0.1	106.2	107.6	28.500	1.6	0.4	0.0	−143.3
32.333	3.2	0.7	95.2	105.2	28.333	1.4	0.0	−24.7	156.2
32.167	1.8	0.6	−112.9	65.5	28.167	1.7	0.0	29.0	28.8
32.000	1.6	0.1	−162.0	17.2	28.000	1.8	1.3	98.4	−35.9
31.833	1.9	0.5	−5.6	5.0	27.833	2.7	0.9	98.3	−58.6
31.667	1.7	0.4	−51.6	−82.5	27.667	3.1	1.7	107.8	−62.3
31.500	1.4	0.1	−56.4	118.5	27.500	3.3	2.4	−55.4	−78.4
31.333	1.7	0.1	−75.6	101.2	27.333	2.8	1.3	41.6	−111.9
31.167	1.3	1.0	−119.8	104.9	27.167	4.2	0.1	23.2	−136.3

(d) Q_1 tide.

latitude	U_{max}	U_{min}	θ_{max}	Θ	latitude	U_{max}	U_{min}	θ_{max}	Θ
35.000	1.0	0.1	−49.7	−63.5	31.000	1.9	1.1	27.4	1.4
34.833	1.4	0.3	22.9	−4.9	30.833	1.8	1.4	36.8	0.9
34.667	0.6	0.2	8.5	17.7	30.667	1.7	1.0	144.7	−25.9
34.500	1.7	0.8	94.7	88.4	30.500	1.4	0.3	144.0	−30.8
34.333	3.6	1.7	−139.2	61.8	30.333	1.7	0.3	−140.7	46.8
34.167	4.0	0.2	−133.5	48.0	30.167	1.7	0.1	−93.8	88.8
34.000	2.3	0.2	−159.7	22.5	30.000	2.0	0.6	−81.7	83.2
33.833	2.6	0.6	162.9	−66.7	29.833	1.8	0.4	−53.2	111.3
33.667	3.5	1.0	166.8	−102.7	29.667	2.6	0.4	−36.4	153.7
33.500	3.5	0.7	162.1	−144.2	29.500	1.8	0.7	−8.8	179.9
33.333	2.7	1.8	171.4	−151.8	29.333	0.4	0.3	0.6	−152.3
33.167	3.4	1.3	54.8	−129.9	29.167	0.4	0.1	165.5	124.2
33.000	3.8	1.1	66.2	−113.7	29.000	1.5	0.0	−131.2	−101.9
32.833	3.8	1.6	79.5	−107.3	28.833	1.5	0.2	−124.8	160.1
32.667	2.6	0.5	108.7	−77.5	28.667	1.5	1.3	−53.8	−169.0
32.500	2.0	0.9	146.2	−38.9	28.500	0.8	0.5	−120.4	−167.7
32.333	1.5	0.3	−149.2	21.1	28.333	2.1	0.1	−154.5	110.7
32.167	1.1	0.3	−106.6	−2.9	28.167	2.4	0.0	−142.5	−147.2
32.000	0.8	0.4	169.5	0.8	28.000	2.5	0.6	−146.4	139.8
31.833	1.3	0.7	−179.3	3.3	27.833	1.1	0.8	−154.2	141.0

latitude	U_{max}	U_{min}	θ_{max}	Θ	latitude	U_{max}	U_{min}	θ_{max}	Θ
31.667	0.9	0.3	144.3	117.4	27.667	0.6	0.2	-103.2	177.9
31.500	1.5	0.6	141.7	172.4	27.500	1.0	0.2	166.9	59.8
31.333	1.4	0.8	99.5	59.2	27.333	1.3	1.1	127.6	78.1
31.167	1.6	0.1	34.8	33.6	27.167	1.3	0.4	94.4	83.4

References

Candela, J., R.C. Beardsley, and R. Limeburner, 1992 : Separation of tidal and subtidal currents in ship-mounted acoustic Doppler current profiler observations, *J. Geophys. Res.*, **97**(C1), 769-788.

Dowd, M. and K.R. Thompson, 1996 : Extraction of tidal streams from a ship-borne acoustic Doppler current profiler using a statistical-dynamical model, *J. Geophys. Res.*, **101**(C4), 8943-8956.

Dronkers, J.J., 1964 : *Tidal computations in rivers and coastal waters*, North Holland, Amsterdam, 518pp.

Foreman, M.G.G. and H.J. Freeland, 1991 : A comparison of techniques for tide removal from ship-mounted acoustic Doppler measurements along the southwest coast of Vancouver Island, *J. Geophys. Res.*, **96**(C9), 17007-17021.

Geyer, W.R., and R. Signell, 1990 : Measurements of tidal flow around a headland with a shipboard acoustic Doppler current profiler, *J. Geophys. Res.*, **95**(C3), 3189-3197.

Hanawa, K., Y. Yoshikawa and T. Taneda, 1996 : TOLEX-ADCP monitoring, *J. Geophys. Res.*, **23**(18), 2429-2432.

Howarth, M.J. and R. Proctor, 1992 : Ship ADCP measurements and tidal models of the North Sea, *Continental Shelf Res.*, **12**(5/6), 601-623.

Marine Safety Agency, 1992 : Document number 742, 267pp. (in Japanese)

Matsumoto, K., M. Ooe, T. Sato and J. Segawa, 1995 : Ocean tide model obtained from TOPEX/POSEIDON altimetry data, *J. Geophys. Res.*, **100**(12), 25319-25330.

Mäunchow, A., R.W. Garvine, and T.F. Pfeiffer, 1992 : Subtidal currents from a shipboard acoustic Doppler current profiler in tidally dominated waters, *Contineatal Shelf Res.*, **12**(4), 499-515.

National Oceanic and Atmospheric Administration, 1995 : TerrainBase, Worldwide digital terrain data, Documentation manual, CD-ROM Release 1.0.

Odamaki, M., 1981 : A new trial on the harmonic analysis for short period observation of tide and tidal current, using the least square method, *Rep. Hydrogr. Res.*, No. 16, 71-82. (in Japanese)

Rikiishi, K., 1982 : Tidal analysis of an equally or randomly spaced record with small number of data samples, *J. Oceanogr. Soh. Japan*, **38**, 373-384.

Schwiderski, E.W., 1979 : On charting global ocean tides, *Rev. Geophys. Space Phys.*, **18**(1), 243-268.

Shum, C.K., P.L. Woodworth, O.B. Andersen, G.D. Egbert, O. Francis, C. King, S.M. Klosko, C. Le Provost, X.Li, J-M Molines, M.E. Parke, R.D. Ray, M.G. Schlax, D. Stammer, C.C. Tierney, P. Vincent, and C.I. Wunsch, 1997 : Accuracy assessment of recent ocean tide models, *J. Geophys. Res.*, **102**(C11), 25173-25194.

Simpson, J.H., E.G. Mitchelson-Jacob, and A.E. Hill, 1990 : Flow structure in a channel from an acoustic Doppler current profiler, *Continental Shelf Res.*, **10**(6), 589-603.

Yoshida, T., S. Sugimoto, and T. Kuragano, 1997 : Production of ocean current grid data, *Weather Service Bulletin*, **64** Suppl., 47-60. (in Japanese)

Yoshikawa, Y., 1993 : A study on structure and variability of the Kuroshio system based on TOLEX XBT/ADCP monitoring, Doc.Thesis, Tohoku University, 100pp. (in Japanese)